Cite this: DOI: 00.0000/xxxxxxxxxx

Electrophoretic interactions governed active-passive assembly based on light-driven micromotors†

Linlin Wang,[a] and Juliane Simmchen*[a]

Received Date
Accepted Date

DOI: 00.0000/xxxxxxxxxx

Non-equilibrium dynamic assembly attracts considerable attention due to the possibility of diverse structures formation. Especially, light-driven micromotors display remarkable prospects for self-assembly with passive surrounding particles. However, due to the complexity of the system, it remains unclear whether the phoretic or hydrodynamic interactions govern the assembly and is not able to decouple the interactions. Here, for light-driven Au@TiO_2 micromotors, we investigate the origin of the main forces driving particle and causing the interactions between active and passive particles. We correlate precise experimental measurements of the photochemical reaction rate with the observed speed of Au@TiO_2 micromotors and conclude that the dominant propulsion mechanism of the active particle is self-electrophoresis based on the self-generated H^+ gradient. In addition, by adding salt, the dependence of the swimming behaviour on salt concentration confirms the motion mechanism. With the implication of the motion mechanism, we find that the chemical resulting electrophoretic interactions govern the assembly of active-passive particles, especially dominant for the significant size of rafts formation. However, the final assembly is the result of the coupling of all interactions, including the diffusiophoretic, electrophoretic, hydrodynamic and electroosmotic interactions, and it is impossible to prior evaluate whether they will add up or diminish each other. Therefore, a complex model including all interactions is highly required to study the motion and the interactions in the future.

1 Introduction

Over the past decades, artificial active matter has stimulated extensive research efforts due to its ability to emulate biological systems.[1–5] In biology, the presence of an active agent frequently influences the behaviour of larger, hierarchically organized structures, enabling the resulting materials or tissues to fulfill certain tasks. Concerning the synthetic analogues, the understanding is still in its infancy, as the engineering of intelligent materials based on the resulting interactions. It has been observed in different systems that upon an encounter of an active particle with micron-sized colloids of the same size level, out-of-equilibrium dynamic assembly can form different structures.[2,6–9] The difficulty in understanding and modeling this behaviour arises from a large number of factors, the first being a general lack of agreement on the precise origin of the driving force even for the most simple model swimmers. Different swimming mechanisms have been postulated (pressure difference, concentration gradient leading to a diffusiophoretic force, additional electric fields).[10–13] As the essence of their existence, a model simplifies the reality for the sake of capturing it and thereby assigns different importance to different parameters. However, due to the complexity of the system, it is not always easy to judge where simplifications are required and where they oversimplify interactions between active and passive systems depending on the underlying motion mechanism of active swimmers.[2]

The active-passive assembly has been experimentally observed with chemically propelled Pt@SiO_2 active particles mixed with passive SiO_2 particles and studied by theory.[7] By now, most reported systems were light-driven to enable the control between active and inactive states of the micromotor. Initially, Singh *et al.* observed TiO_2@SiO_2 actives to form isotropic assemblies with passive particles.[6] There is an ongoing discussion on which interaction dominates the assembly behaviour.[14,15]The team around Holger Stark focuses on phoretic interactions, neglecting hydrodynamic interactions primarily,[16] while Uspal recognized that both chemical and hydrodynamic fields play a role, using a continuum model.[7]

For our light-driven Janus Au@TiO_2 microswimmers, reaching speeds of more than 200 μm/s, we demonstrated that the hydrodynamic interactions need to be taken into account for the raft formation in the previous study.[17] There are three phases during the raft formation: free motion of active swimmer, spinning motion of an active-passive pair and pronounced rafting (see Figure S1). The phenomenon of spinning pair formation and the large magnitude of rafts have not been observed in similar systems[6] which points towards a hydrodynamics origin. The study clearly showed that the hydrodynamics induced by active swimmers control the spinning behaviour and enable forming minor size raft via implementing dominant hydrodynamics in a squirmer model using the Smoothed Profile Method and simplified phoretic interactions. However, despite the excellent agreement for the spinning

[a] *Department of Physical Chemistry, TU Dresden, Zellescher Weg 19, 01069 Dresden, Germany E-mail: juliane.simmchen@tu-dresden.de*

† Electronic Supplementary Information (ESI) available: [details of any supplementary information available should be included here]. See DOI: 10.1039/cXsm00000x/

‡ Additional footnotes to the title and authors can be included *e.g.* 'Present address:' or 'These authors contributed equally to this work' as above using the symbols: ‡, §, and ¶. Please place the appropriate symbol next to the author's name and include a `\footnotetext` entry in the the correct place in the list.

state, this approach fails to reproduce the magnitude of larger rafts (more than 50 passive particles by one active motor), and the stability of a passive particle's position within a raft. This result implies that in our previous model, phoretic interactions are too simplified in the simulations.

In the current work, we investigate the origin of the main phoretic forces driving the particle and causing interactions. To reveal the role of different solute molecules, we measure the oxygen production and correlate it to the predicted outcome of different possible motion mechanisms (self-diffusio-/electrophoresis). Finding that uncharged interactions cannot account for the high observed speeds, we implement the resulting electric field into the active-passive interactions and find quantitative agreement.

2 Results and Discussion

2.1 Motion Mechanisms

Dominant motion mechanism: self-electrophoresis

In general, propulsion mechanisms are still highly disputed for most types of microswimmers. This is especially pronounced for photocatalytic ones because of the unclear role of the field generated by charge separation.[6,18] When our active Janus Au@TiO_2 particles are irradiated with UV light, matching the band gap of the material, the electrons are excited to the conduction band and transfer to Au cap, thus being involved in the reduction reaction of H_2O_2, while holes remain in the valence band and participate in the oxidation of H_2O_2 at the TiO_2 hemisphere:

$$TiO_2\ side: H_2O_2 + 2h^+ \longrightarrow O_2 + 2H^+$$

$$Au\ side: H_2O_2 + 2H^+ + 2e^- \longrightarrow 2H_2O$$

$$Overall\ reaction: 2H_2O_2 \longrightarrow 2H_2O + O_2$$

Two gradients form during the reaction process: O_2 and H^+ but their contributions to the actual motion are disputable. Therefore, two possible mechanisms for self-propulsion are considered here: self-diffusiophoresis based on an uncharged solute O_2 gradient, and self-electrophoresis due to the electric potential gradient resulting from the charged H^+ gradient. In the following section, we will discuss these two mechanisms briefly, following the theoretical lines of Anderson's diffusiophoresis equation[10] and Smoluchowski electrophoresis equation which we use to predict speeds to evaluate which gives better agreement with our experimentally measured speeds.

In the self-diffusiophoresis model (Figure 1A), within a thin interfacial layer (labelled as the interaction zone with the red circle in the scheme), interactions (attraction or repulsion)[10,19] between the solute molecules and particle surface induces a tangential gradient osmotic pressure gradient in the interfacial region when there is a self-generated gradient of O_2, which leads to a slip velocity (v_s).[11,20,21]

For example, here we assume repulsive interactions between O_2 molecules and the surface of particle, resulting in fluid flows (v_s) toward higher O_2 concentration from Au side to TiO_2 side, and consequently the particle moves in the opposite direction of the fluid flow (toward the Au side). The speed of the swimmer can be calculated following an approach by:

$$V = b\nabla Y_\infty \tag{1}$$

where b is slip-velocity coefficient which can be varied over the material surface property, and ∇Y_∞ is O_2 gradient.[10]

For self-electrophoresis (see scheme in Figure 1B), within the interfacial layer around the particle, the negative charge on the particle's surface is balanced by the H^+ space charge. The gradient of charged H^+ induces an electric field from TiO_2 side to Au side. This self-generated electric field acts on the H^+ space charge, producing an electrical body force on the fluid, thus leading to the fluid's flow toward the Au side. As a result, the negatively charged Janus Au@TiO_2 particles undergo an electrophoretic transport toward TiO_2 side. The speed based on self-electrophoresis is estimated by the Smoluchowski equation:

$$V_{ep} = \frac{\varepsilon_r \varepsilon_0 \zeta}{\eta} E \tag{2}$$

with where ε_r is the dielectric constant of the solvent, ε_0 is the absolute permittivity, η is the dynamic viscosity of the solvent, ζ is the zeta potential of particle and E is the self-generated electric field.

To evaluate whether electro- of diffusiophoretic processes are dominant in the swimmer's propulsion, the oxygen evolution rate is required for the speed values, determined using equation 2 and 1 compared to the experimentally measured speed values. The O_2 generation rate represents a very intricate measurement, which was accessed initially using electrochemistry.[22,23] However, this elegant approach can not be performed on particles directly, so similar thin-film materials were used instead previously,[13] which does not give realistic estimates for photoactive systems. Measurements of the displaced water volume by gas evolution can include the specifications of colloidal systems, but also considerations for photoactivated systems are lacking here.[24] The precise measurement of the O_2 generation is crucial here, as is the knowledge of the underlying amount of particles. Here, we developed a Janus Au@TiO_2 colloid monolayer with well-known dimensions (see SEM image Figure S2) to determine the amount of particle and then in contact with the different concentrations of H_2O_2 solution and irradiated with UV LED used in motion experiments for measurement of oxygen generation rate per particle per second. More details on the setup of oxygen measurement can be found in SI Figure S3 and the experimental section. The experimental oxygen generation rate for different concentrations of H_2O_2 is shown in Figure1C indicated by blue columns.

Using these values in calculations following the relation postulated by Anderson and Smoluchowski, we obtain different speed values for both models. In the following paragraph, we will briefly present exemplary calculations, using the measured oxygen rate at 2.5% H_2O_2, which reaches $2.13 \times 10^{-5}\ (mol/m^2/s)$.

For details on the full calculations please consult the SI; briefly, we calculate the diffusiophoretic speed[10] from the scalar product between coefficient b and the generation rate, resulting in a diffusiophoretic speed of 1.2 Å/s, which is several orders of magnitude smaller than the experimentally measured speed (Figure 1C, yel-

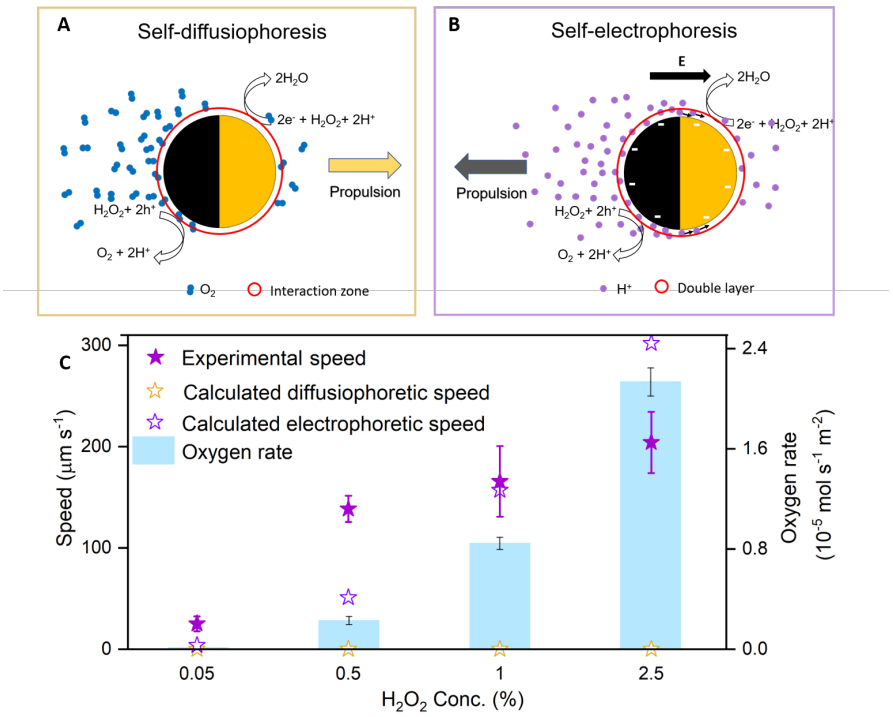

Fig. 1 (A, B) Schematic representations of two possible motion mechanisms: self-diffusiophoresis and self-electrophoresis. (C) Speed and oxygen generation rate of active Au@TiO_2 microswimmers with different H_2O_2 concentrations. The solid purple star represents the experimentally measured speed. The hollow yellow and purple stars represent calculated speed values according to self-diffusiophoretic and self-electrophoretic motion mechanisms. The blue column indicates the oxygen generation rate obtained by the photocatalytic test (details in SI).

low hollow star). Self-electrophoresis requires the Smoluchowski equation for speed calculations, wherein the self-generated electric field is calculated with the method described by ref[25] using the proton flux, which is proportional to the generated oxygen flux (see eq.3 in SI). The estimated speed is around 302 μm/s (Figure 1C, purple hollow star). Comparing both values to the experimentally observed speed of 204 μm/s, we find a much better agreement for the self-electrophoresis model. Therefore, we conclude that self-electrophoresis based on proton flux is the dominant propulsion mechanism for Au@TiO_2 particles. Extending these considerations to other H_2O_2 concentrations (0.05%, 0.5% and 1%), supports this finding (see in Figure 1C).

Proton flux influence

As already considered in the electrophoretic mechanism, the electric field is considered uniform in the above discussion. However, this assumption is an oversimplification. But we can visualize the assumed detailed charge distribution using a COMSOL simulation which accounts for proton transport, space charge and fluid flow to simulate the proton concentration and the electric potential distribution around the particle according to the previous report by Wang *et al.*[22]. It is worth noting that the initial proton concentration in bulk solution is vital for the H^+ gradient simulation. Therefore, we measured the initial pH of different H_2O_2 concentrations (values of pH and initial proton concentration are listed in Table S1) and implemented the obtained data into our COMSOL simulations. With this refined method, we can observe the proton concentration considering that the protons are produced at the TiO_2 side and consumed at Au side, as shown in Figure

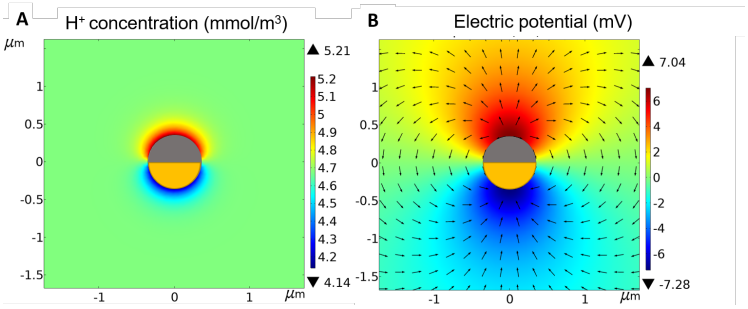

Fig. 2 COMSOL simulation images of proton concentration (A) and electric potential (B) distribution around an active swimmer in 2.5% H_2O_2 solution. The arrows in B represent the electric field direction.

2A. The resulting non-homogeneous electric potential and electric field are illustrated in Figure2B. COMSOL also solves for the swimmers speed using the proton flux obtained from our experimental O_2 generation rate measurement, resulting in a simulated speed of about 239 μm/s, which is slightly smaller than the analytically calculated speed (302 μm/s). However, it is closer to our experimental speed (204 μm/s), showing that accounting for coupling effects of proton concentration, electrostatic potential, and the flow field is more precise. The detailed simulated, calculated and experimental speed is listed in Table S2.

According to the Smoluchowski equation, the electrophoretic velocity is proportional to the electric field, which in our case is mainly determined by the proton flux. Experimentally, we can control the proton flux by changing fuel concentration and light

intensity. For example, by increasing the H_2O_2 concentration from 0.05% to 2.5%, the reaction rate is accelerated, which also increases the proton gradient, electric field and thus speed (see COMSOL simualtion Figure S5, S6 and Video S1). Also, modulating UV light intensity can modify the number of photons participating in the reaction and thereby the proton flux. Modulating the UV light intensity from 2% to 100% and keeping the H_2O_2 concentration fixed at 0.5%, the velocity increases from 24 to 138 μm/s, as shown in Figure S7 and Video S2. However, this parameter is not accounted for in the simulation.

Salt influence

An established test for electrophoretic motion is increasing the salt concentration in the medium, which significantly affects the electric field and thereby influences the particle's speed and behaviour.[12] Adding salt to the bulk solution affects the conductivity (k) of the solution, which, according to Ohm's Law (E = J/k), is inversely proportional to the electric field. This leads to reduced speeds for the self-electrophoretic motors.[23,26,27] In our experiment, the speed decreases after adding KCl solutions (the final concentrations varying from 0 to 1.25 mM), as shown in Figure S8 and Video S3. The conductivities increase by almost two orders of magnitude from 0.0078 to 0.6000 mS/cm. As a secondary effect, the rise in ionic strength decreases the Debye length due to the screening effect of ions cloud on the net charge of the particle.[12] This decreases the zeta potential of the particles, which again reduces the speed. Detailed values of the conductivity and zeta potential are listed in Table S3. These assumptions are confirmed especially by the fact that the Janus particles are stuck on the substrate at the highest salt concentration, 0.125 M.

2.2 Active-Passive Interactions

As we described and explored elsewhere,[1,17] our active Au@TiO_2 active swimmers start forming rafts when they encounter passive particles (2 μm SiO_2). We found that the hydrodynamic component of the interactions is crucial, especially in the initial state.[17] However, it is not possible for larger raft formation with dominant hydrodynamic interactions. To reduce the hydrodynamic influence induced by the motion of active particle, an active particle is immobilized on the substrate. The passive particles are still attracted by the fixed active particles and form raft, demonstrating the critical role of phoretic interactions (see Video S4). Here, we want to explore the influence of the electric field generated by the proton gradient to see whether we can explain the remaining open points, such as the extension of the rafts and position stability. The highly negatively charged SiO_2 particles (zeta potential, 40 mV) immersed in the electric field generated by the active swimmer undergo the electric body force, thus showing electrophoretic motion toward the active swimmer as shown in Figure 3A scheme. In this case, the interactions between active and passive refer to electrophoretic interactions. These rafts are characterized by a crystalline order of the passive particles and remain motile, even though the average speed decreases, as shown in Figure 3B and Video S5. Because the passive particles slow down active swimmers' speed along with the assembly, the chemical and electric fields become stronger compared to the freely moving case, inducing crystallinity. The slowing down of the active particle can be explained by the increased drag radius (r) of the assembly. Since drag force (F) is equal to the constant driving force, the speed decreases with the increased r, according to Stokes' Law:

$$F = 6\pi\eta r v \tag{3}$$

where η is the dynamic viscosity of the medium, r is the effective drag radius, and v is the speed. The speed behaves inversely proportional to the assemblies' effective radius.

The slowing down effect reduces the area covered by the gradient and therefore leads to a more pronounced gradient of protons (and oxygen). This leads to a noteworthy phenomenon occurring during the raft formation process: the enlargement of the interaction range. At the earlier stage of the raft formation, passive particles further away than 3 μm from the active particle are not attracted. In contrast, after a certain time with the larger raft, they can be incorporated into the raft (see Figure 3C). The more pronounced proton gradients induces a significant electric potential gradient. Additionally, the passive particles occupy the volume at the front of the swimmer, which hinders the diffusion of protons and thereby increases the gradient (and electric field) further. To confirm and verify whether these observations are consistent with our postulation, we perform COMSOL simulations of active particles assembled with different numbers of (0, 1, 2, 4, 8, 16) SiO_2 particles according to experimental results in Figure 3D. We can see that a more pronounced proton gradient is generated (see in Figure S9). That means that adding up to the stiffer gradient due to the less motility of the swimmer and the accumulation of passive particles, the electric potential is enhanced (Figure 3E), thus extending the interaction range even further (Figure S10).

Salt influence on active-passive interactions

As we discussed before, adding salt is the most common test employed to verify the impact of electric fields. Extrapolating this to active-passive systems, the weakened electric field also weakens the electrophoretic interactions, and the raft size is expected to reduce by adding KCl in H_2O_2 solution, which is confirmed in Figure 4A-C (images from Video S6).

Under the shielding effect of salt, the charge interaction is increasingly limited until in a 1.25×10^{-3} M KCl solution, the swimmer can not form assemblies anymore but still shows spinning behaviour. With even higher salt concentration, Janus particles stop free motion and get stuck on the substrate (Figure 4E-F, red circles), which can be explained by the more minor repulsive interactions between Janus particles and substrate due to the shorter Debye length. In diluted H_2O_2 solution containing 0.125 M KCl, not only Janus particles but also SiO_2 particles are stuck on the glass slide. Even though adding salt does not allow us to decouple the individual hydrodynamics and chemical resulting electric fields effects, it still points toward the high significance of the electrochemical fields.

Proton flux influence on active-passive interactions

Correspondingly to the increased activity observed when active particles are placed in higher fuel concentrations, larger assemblies are formed. As illustrated in Figure 5A and B, when in-

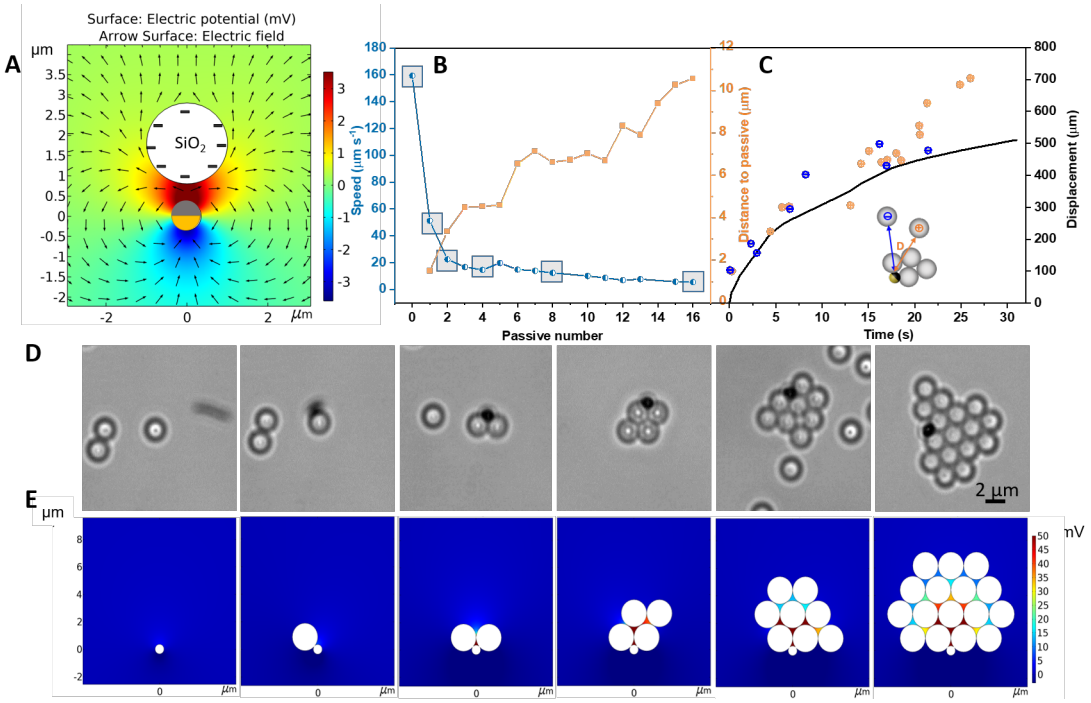

Fig. 3 (A) Scheme of the electrophoretic interactions between active and passive particles: One negatively charged SiO_2 particle is immersed in the electric field induced by an active swimmer and attracted toward the active swimmer. (B) The active swimmer slows down along with the assembly (blue line). Meanwhile, the attractive distance to passive particles increases, demonstrating that the range of the interactions is influenced by attracted passive particles (orange line). (C) Attractive (orange circle) and non-attractive (blue circle) distance. At the stage of a small raft, the attractive distance is only around 1.8 μm, while for larger rafts, the attractive range is around 10 μm. (D, E) Microscope images and corresponding electric potential distribution when different numbers of passive particles assemble at the front of the active swimmer.

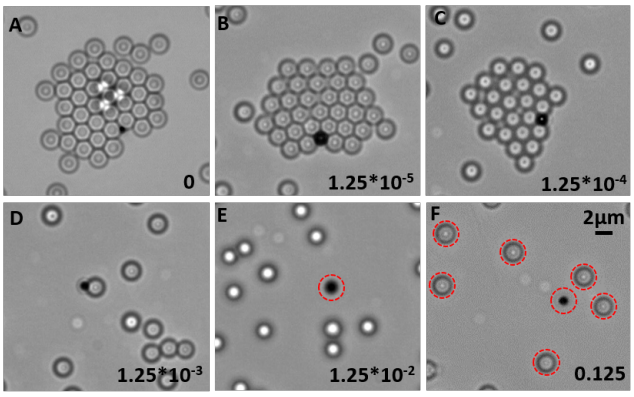

Fig. 4 Microscope images of active-passive rafts in 0.5% H_2O_2 solution containing different concentrations of KCl (0-0.125 M). The size of rafts decreases with adding KCl firstly. Then with even higher salt concentration, the active and passive particles get stuck on the substrate. The red circles in the images represent the stuck particles.

creasing the peroxide concentration from 0.05% to 0.5%, 1% and 2.5%, the number of collected SiO_2 increase (also see Video S7). For a H_2O_2 concentration of 0.05%, the amount of attracted SiO_2 with one swimmer is around 20, accumulated in 3 shells of particle layers. This increases to 52 assembled particles in 7 shells in 2.5% H_2O_2. As explained for the purely active particles, the activity can also be modulated by UV light intensity. The range of the interactions and thus the raft size also can be modulated in this way (see Figure S7 and Video S8). The correlation that with higher UV light intensity, also the raft size increases confirms our conjectures.

Figure 5A displays the few moments during the assembly process along with active motion in 1% H_2O_2. After around 2 min, we observed an interesting phenomenon: the raft size achieves a stable state. A closer look at the details reveals a particular asymmetric hexagon crystal pattern that occurs in all cases with different fuel concentrations and light intensities in our experiments (see Figure 5B and Figure S7). Fischer's group has observed other perfect symmetric patterns (square, pentagonal, hexagonal, and heptagonal) forming around the flipped active particles.[6]. However, in our case, the active swimmers move directionally without flipping out of the swimming position; the chemical field around the active particle is asymmetric, which allows the assembly of a asymmetric raft, offering the potential to form more extensive, functional materials.

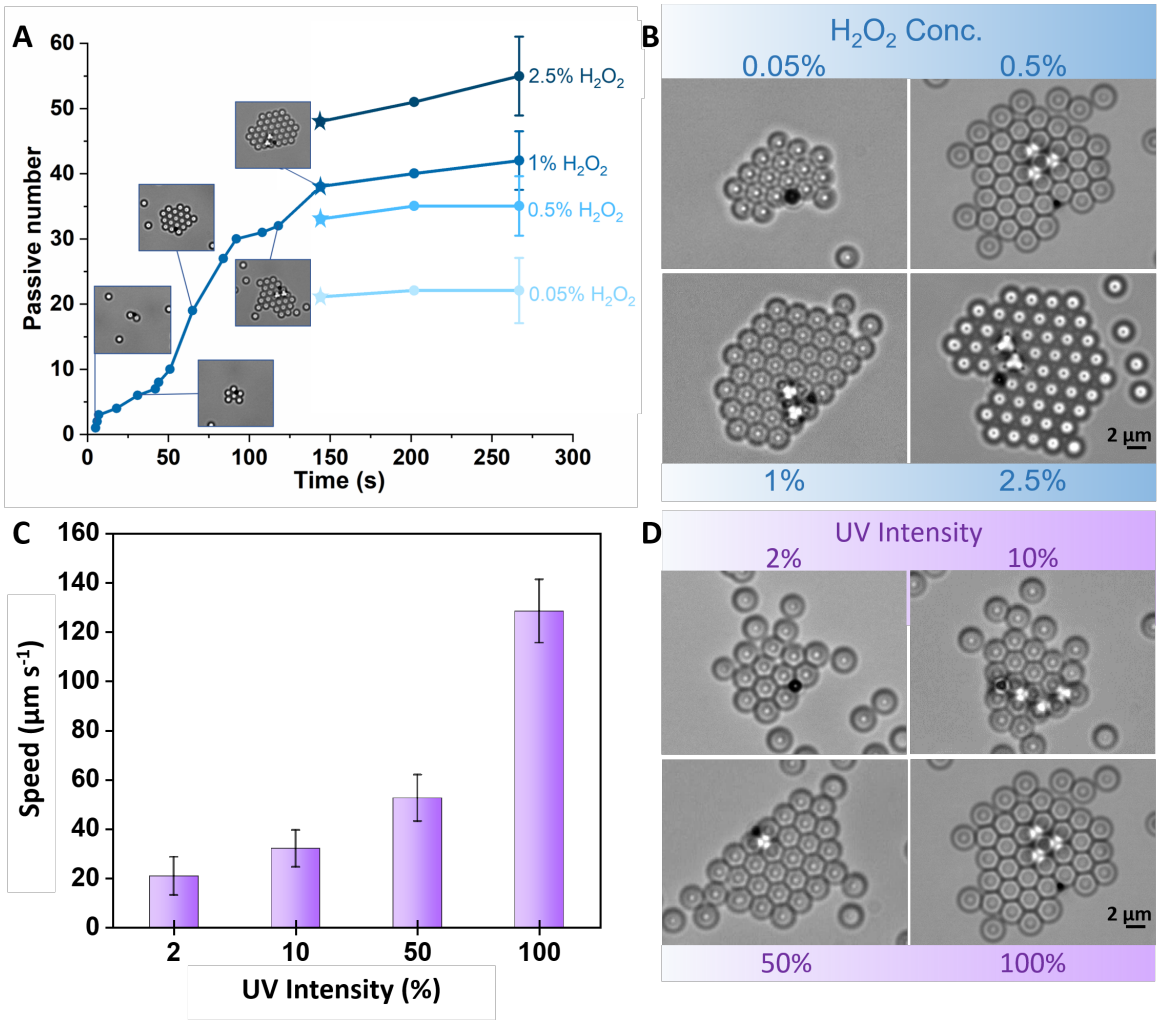

Fig. 5 (A) The microscope images illustrating that the size of the raft increases firstly along with motion time and reaches a stable plateau state at 1% H_2O_2. At other H_2O_2 concentrations (0.05, 0.5 and 2.5%), they show a similar trend. The blue stars represent the moment that the raft size becomes stable. (B) Microscope images of the defined crystallized rafts: With the increase of fuel concentration, the raft size increase.

3 Conclusions

In this work, we correlate the precise experimental oxygen generation rate with the observed motion speed of Au@TiO_2 microswimmers and conclude that the dominant propulsion mechanism is self-electrophoresis. Moreover, the dependence of the swimming behaviour on salt concentration confirms that. Subsequently, we investigate the role of the self-generated electric fields by implementing a COMSOL model. Furthermore, we extend our considerations to active-passive particle mixtures, where, similar to pure active microswimmers, we find that the dominant electrophoretic interactions align with the chemical effects that cause them. They can be used to explain the raft formation, the dimensions of the raft and the enlarged interactions range with passive particles. Additionally, we could confirm that the salt influence holds true also for the assembly capacity of these Au@TiO_2 microswimmers. Moreover, considering different fuel concentrations, we find good agreement for individual rafts' size and swimming speed, which we can reproduce in our COMSOL model and also confirm experimentally, using different light intensities.

However, other interactions, such as diffusiophoretic, hydrodynamic and electroosmotic interactions, also contribute to motion and interactions, which should be considered together. The final assembly is the result of the coupling of these different interactions and we can not a prior evaluate whether they will add up or diminish each other. Therefore, we conclude that a complex model, besides the hydrodynamic and the electrophoretic interaction, including all other interactions, is required to evaluate the active motion and the interactions it causes with the surroundings in order to pave the way for the active assembly of functional materials.

4 Experimental Section

Materials and Reagents

Titanium(IV) iso-propoxide (TTIP) was obtained from Alfa Aesar Co. Ltd. Dodecylamine (DDA), 30 wt% H_2O_2 and 5 wt% 2 μm SiO_2 suspension in water were purchased from Sigma Aldrich. SiO_2 suspension was diluted to 0.05% for experiments. Methanol and acetonitrile were purchased from VWR and used without further treatment.

Preparation of Au@TiO_2 Particles

700 nm TiO_2 particles were synthesized via the sol-gel method.[1] 105 mL of methanol and 45 mL of acetonitrile were mixed in a 250 mL round bottom flask. 180 μL of DI water was added to the mixture. 0.28 g of DDA was added to the flask and stirred for 10 min. Then 1 mL of TTIP was dropped by drop and slowly under magnetic stirring. The mixture was stirred for 12 h and then particles were collected by centrifugation. Subsequently, the particles were washed with methanol three times and dried at 60°C for 2 h. The TiO_2 particles were obtained after calcination at 600°C for 2 h under a nitrogen atmosphere. To obtain Janus Au@TiO_2 particles, the monolayer of TiO_2 on a glass substrate was first prepared by the drop-casting of TiO_2 ethanol suspension. Then 30 nm of Au layer was coated on the surface of the monolayer by thermal deposition. In the end, the Janus Au@TiO_2 particles were detached from the substrate by ultrasonication.

Record of Pure Active Au@TiO_2 Microswimmers Movement and Active-Passive Colloids Rafts Formation

The motion of active Janus Au@TiO_2 and the raft formation with passive SiO_2 particles were recorded by an optical microscope (Carl Zeiss Microscopy GmbH, Germany). An UV LED (385 nm) with adjustable intensity was used as UV source; more details on the intensities are listed here[28]. The videos were recorded with a frame rate of 40 fps. For the test of pure active Au@TiO_2 swimmers motion, 5 μL Janus particles and 5 μL H_2O_2 solution were dropped on a clean glass substrate. For active-passive raft formation measurements, 5 μL Janus particles, 5 μL 0.05% SiO_2 and 10 μL H_2O_2 were added.

Video Analysis

Videos were analyzed with Fiji[29] for speed measurements and data was evaluated in Origin. The distance of passive particles to active swimmers was measured manually using image analysis with Fiji.

Oxygen Generation Measurement

The drainage method based on the setup shown in Figure S3 was used for the oxygen generation rate measurements of Au@TiO_2 particles. A nice monolayer of TiO_2 (see SEM image in Figure S2) on 24×3 mm glass slide was prepared by a Langmuir Blodgett device. Then a layer of Au with 30 nm was deposited on the monolayer. The total amount of Au@TiO_2 particles was determined via SEM image analysis. The slide with particles was dipped in a cuvette with H_2O_2 solution for 15 min. The UV light from the microscope was switched on and then the oxygen was collected by water displacement with a small syringe cylinder for 30 min, measuring the gas volume. Finally, the oxygen generation rate (mole per second per particle) was calculated.

Conflicts of interest

There are no conflicts to declare.

Acknowledgements

We thank the Volkswagen Foundation for the Freigeist fellowship (grant number 91619). LL. Wang acknowledges financial support from China Scholarship Council. We acknowledge Ian P. Madden and Prof. Erik Luijten for the discussion of the results. We thank ZY. Xiao for helping with COMSOL simulation.

Notes and references

1 L. Wang, A. Kaeppler, D. Fischer and J. Simmchen, *ACS applied materials & interfaces*, 2019, **11**, 32937–32944.
2 L. Wang and J. Simmchen, *Condensed Matter*, 2019, **4**, 78.
3 X. Guo, Y. Wang, F. Mou, Q. Xie, S. Su, C. Chen and J. Guan, *Journal of Materials Chemistry C*, 2022, **10**, 5079–5087.
4 J. Zhang, J. Song, F. Mou, J. Guan and A. Sen, *Trends in Chemistry*, 2021, **3**, 387–401.
5 J. Zhang, F. Mou, Z. Wu, J. Song, J. E. Kauffman, A. Sen and J. Guan, *Nanoscale Advances*, 2021, **3**, 6157–6163.

6 D. P. Singh, U. Choudhury, P. Fischer and A. G. Mark, *Advanced Materials*, 2017, **29**, 1701328.

7 J. Katuri, W. E. Uspal, M. N. Popescu and S. Sánchez, *Science Advances*, 2021, **7**, eabd0719.

8 Y. Gao, F. Mou, Y. Feng, S. Che, W. Li, L. Xu and J. Guan, *ACS applied materials & interfaces*, 2017, **9**, 22704–22712.

9 W. Wang, W. Duan, A. Sen and T. E. Mallouk, *Proceedings of the National Academy of Sciences*, 2013, **110**, 17744–17749.

10 J. L. Anderson, *Annual review of fluid mechanics*, 1989, **21**, 61–99.

11 J. L. Moran and J. D. Posner, *Annual Review of Fluid Mechanics*, 2017, **49**, 511–540.

12 A. Brown and W. Poon, *Soft matter*, 2014, **10**, 4016–4027.

13 X. Lyu, X. Liu, C. Zhou, S. Duan, P. Xu, J. Dai, X. Chen, Y. Peng, D. Cui, J. Tang *et al.*, *Journal of the American Chemical Society*, 2021, **143**, 12154–12164.

14 B. Liebchen and H. Löwen, *The Journal of chemical physics*, 2019, **150**, 061102.

15 B. Liebchen and A. K. Mukhopadhyay, *Journal of Physics: Condensed Matter*, 2021, **34**, 083002.

16 J. Stürmer, M. Seyrich and H. Stark, *The Journal of chemical physics*, 2019, **150**, 214901.

17 I. P. Madden, L. Wang, J. Simmchen and E. Luijten, *Small*, 2022, 2107023.

18 R. Dong, Q. Zhang, W. Gao, A. Pei and B. Ren, *ACS Nano*, 2016, **10**, 839–844.

19 J. L. Anderson and D. C. Prieve, *Separation and Purification Methods*, 1984, **13**, 67–103.

20 A. Ajdari and L. Bocquet, *Physical review letters*, 2006, **96**, 186102.

21 R. Golestanian, T. Liverpool and A. Ajdari, *New Journal of Physics*, 2007, **9**, 126.

22 W. Wang, T.-Y. Chiang, D. Velegol and T. E. Mallouk, *Journal of the American Chemical Society*, 2013, **135**, 10557–10565.

23 W. F. Paxton, P. T. Baker, T. R. Kline, Y. Wang, T. E. Mallouk and A. Sen, *Journal of the American Chemical Society*, 2006, **128**, 14881–14888.

24 A. Nsamela, P. Sharan, A. Garcia-Zintzun, S. Heckel, P. Chattopadhyay, L. Wang, M. Wittmann, T. Gemming, J. Saenz and J. Simmchen, *ChemNanoMat*, 2021, **7**, 1042–1050.

25 T. R. Kline, J. Iwata, P. E. Lammert, T. E. Mallouk, A. Sen and D. Velegol, *The Journal of Physical Chemistry B*, 2006, **110**, 24513–24521.

26 J. L. Moran and J. D. Posner, *Physics of Fluids*, 2014, **26**, 042001.

27 W. Wang, X. Lv, J. L. Moran, S. Duan and C. Zhou, *Soft Matter*, 2020, **16**, 3846–3868.

28 S. Heckel, M. Wittmann and J. Simmchen, 2021.

29 J. Schindelin, I. Arganda-Carreras, E. Frise, V. Kaynig, M. Longair, T. Pietzsch, S. Preibisch, C. Rueden, S. Saalfeld, B. Schmid *et al.*, *Nature methods*, 2012, **9**, 676–682.